Synthesis of $[Ru(phen)_2dppz]^{2+}$-Tethered Oligo-DNA and Studies on the Metallointercalation Mode into the DNA Duplex

Dimitri Ossipov, P. I. Pradeepkumar, Melcer Holmer, and Jyoti Chattopadhyaya*

Contribution from the Department of Bioorganic Chemistry, Box 581, Biomedical Center, University of Uppsala, Sweden

Received November 16, 2000

Abstract: To explore the binding properties of $[Ru(phen)_2dppz]^{2+}$ complex (phen = 1,10-phenanthroline, dppz = dipyrido[3,2-a:2′,3′-c]phenazine) in a sequence-specific manner in DNA duplex, it was tethered *through the dppz ligand* to a central position as well as both at the 3′- and 5′-ends of oligodeoxyribonucleotide (ODN). The middle $[Ru(phen)_2dppz]^{2+}$-ODN tethered was resolved and isolated as four pure diastereomers, while the 3′- or 5′-$[Ru(phen)_2dppz]^{2+}$-ODNs were inseparable on RP-HPLC. Thermal stability of the (Ru^{2+}-ODN)• DNA duplexes is found to increase considerably (ΔT_m = 12.8−23.4 °C), depending upon the site of the covalent attachment of the tethered $[Ru(phen)_2dppz]^{2+}$ complex, or the chirality of the $[Ru(phen)_2dppz]^{2+}$-linker tethered at the middle of the ODN, compared to the unlabeled counterpart. Gross differences in CD between the $[Ru(phen)_2dppz]^{2+}$-tethered and the native DNA duplexes showed that the global duplex conformation of the former has considerably altered from the B-type, but is still recognized by DNase I. The thermal melting studies, CD measurements, as well as DNase I digestion data, are interpreted as a result of intercalation of the dppz moiety, which is realized by threading of the $Ru(phen)_2$ complex part through the DNA duplex core. DNase I footprinting with four diastereomerically pure middle ($[Ru(phen)_2dppz]^{2+}$-ODN)• DNA duplexes furthermore showed that the tethered $[Ru(phen)_2dppz]^{2+}$-linker chirality dictates the stereochemical accessibility of various phosphodiester moieties (around the intercalation site) toward the cleavage reaction by the enzyme. The diastereomerically pure ruthenium-modified duplexes, with the well-defined π-stack, will be useful to explore stereochemistry-dependent energy- and electron-transfer chemistry to understand oxidative damage to the DNA double helix as well as the long-range energy- and electron-transfer processes with DNA as a reactant.

Introduction

Polypyridyl Ru^{2+} complexes are useful nonradioactive probes for structure elucidation of nucleic acids. They have been found to be valuable as luminescent reporters,[1] DNA/RNA cleaving[2] or cross-linking[3] agents, and also for the study of the long-range energy- and electron-transfer processes through the DNA.[4] The most attractive way to evaluate the binding properties of Ru^{2+} metal complexes with nucleic acids in a sequence-specific manner is to covalently incorporate Ru^{2+} metal complexes into ODNs with a spacer, ensuring a well-defined donor−acceptor distance and geometry. This can be achieved by varying both the attachment site to the ligand of the Ru^{2+} metal complex as well as the linker length, thereby opening the possibility to engineer the mobility as well as the delivery of the Ru^{2+} complex in a stereospecific manner along the double-helical core.

To date, the preparation of Ru^{2+}-containing ODNs is based on either (i) modifying the nucleic acid single-strand after the solid-phase synthesis or (ii) synthesizing the Ru^{2+} complex-derivatized phosporamidite and its subsequent incorporation into the nucleic acid strand during the solid-phase synthesis protocol. In the first approach, the ligand-bearing ODN strand was reacted with bis(polypyridyl)Ru^{2+} to give the desired trischelated complex covalently attached to either the 3′- or 5′-terminus of the probe sequence[5,6] or to an internal nucleotide residue.[7] This also has been achieved by employing an activated ester of tris-(polypyridyl)Ru^{2+} complex to link either to a 5′-alkylamino ODN derivative,[8−10] or to an amino derivative of an internal uracil residue.[11] The 5′-conjugation of Ru^{2+} complex to ODN has been achieved by the postsynthetic modification by the H-phosphonate derivative of the Ru^{2+} complex.[12]

In the second approach, the Ru^{2+}-derivatized phosphoramidites have been used in an automated DNA synthesizer with

(1) Sigel, A.; Sigel, H.; *Probing of Nucleic Acids by Metal Ion Complexes of Small Molecules*; Marcel Dekker Inc.: New York, 1996; Vol. 33, p 678.
(2) Fleisher, M. B.; Waterman, K. C.; Turro, N. J.; Barton, J. K. *Inorg. Chem.* **1986**, *25*, 3549−3551.
(3) Jacquet, L.; Kelly, J. M.; Kirsch-De Mesmaeker, A. *J. Chem. Soc., Chem. Commun.* **1995**, *913*.
(4) Holmlin, R. E.; Dandliker, P. J.; Barton, J. K.; *Angew. Chem., Int. Ed. Engl.* **1997**, *36*, 2714−2730.
(5) Kelly, J. M.; Tossi, A. B.; McConnel, D. J.; OhUigin, C.; Hélène, C.; Le Doan, T. In *Free Radicals, Metal Ions and Biopolymers;* Beaumont, P. C., Deedle, D. J., Parsons, B. J., Rice-Evans, C., Eds.; Richelieu Press: London, 1989; pp 143−156.
(6) Wiederholt, K.; McLaughlin, L. W. *Nucleic Acids Res.* **1999**, *27*, 2487−2493.
(7) Telser, J.; Cruickshank, K. A.; Schanze, K. S.; Netzel, T. N. *J. Am. Chem. Soc.* **1989**, *111*, 7221−7226.
(8) Bannwarth, W.; Schmidt, D.; Stallard, R. L.; Hornung, C.; Knorr, R.; Muller, F. *Helv. Chim. Acta* **1988**, *71*, 2085−2099.
(9) Jenkins, Y.; Barton, J. K. *J. Am. Chem. Soc.* **1992**, *114*, 8736−8738.
(10) (a) Arkin, M. R.; Stemp, E. D.; Pulver, S. C.; Barton, J. K. *Chem. Biol.* **1997**, *4*, 389−400. (b) Nunez, M. E.; Hall, D. B.; Barton, J. K. *Chem. Biol.* **1999**, *6*, 85−97. (c) Wagenknecht, H.-A.; Stemp, E. D.; Barton, J. K. *J. Am. Chem. Soc.* **2000**, *122*, 1−7.
(11) Ortmans, I.; Content, S.; Boutonnet, N.; Kirsch-De Mesmaeker, A.; Bannwarth, W.; Constant, J.-F.; Defrancq, E.; Lhomme, J. *Chem. Eur. J.* **1999**, *5*, 2712−2721.
(12) Meggers, E.; Kursch, D.; Giese, B. *Helv. Chim. Acta* **1997**, *80*, 640−652.

10.1021/ja003985t CCC: $20.00
Published on Web 03/24/2001

enormous flexibility for rapid and straightforward introduction of the Ru^{2+} complex at various sites of ODN.[13−16]

Among the various types of Ru^{2+} complexes studied so far, $[Ru(phen)_2dppz]^{2+}$ is probably the most interesting because it binds extremely strongly to double-stranded DNA ($K = 10^8$ M^{-1})[17] through intercalation of its elongated planar dppz moiety, displaying intense photoluminescence (molecular "light switch").[9,18] Postsynthetic covalent 5′-attachment of $[Ru(phen)_2dppz]^{2+}$ to an ODN has been accomplished by Barton and co-workers,[9,10] and Giese et al.[12] and Barton and co-workers have subsequently used this as specific fluorescent probes[9,12] and cleaving agents ("artificial nucleases")[10] as well as to study long-range electron transfer through a $[Ru(phen)_2dppz]^{2+}$-tethered 15mer DNA duplex.[19] The use of $[Ru(phen)_2dppz]^{2+}$-DNA and $[Ru(diimine)_3]^{2+}$-DNA conjugates, in general, has enabled exploration of different photochemical properties of Ru^{2+} complexes at the target ODN sequences.[20] In all of these conjugation works on tethered $[Ru(phen)_2dppz]^{2+}$, the linker was attached to one of the phen ligands, thereby giving precise preferences to a certain geometry of intercalation vis-à-vis the DNA duplex helix. This unfortunately resulted in only a T_m rise of 3−8 °C.[10a,12]

In this study, we have synthesized $[Ru(phen)_2dppz]^{2+}$-tethered ODNs (as in the 5′-, 3′-, and the middle-modified oligos, **10**, **11**, and **12**, respectively), in which the dppz moiety has been used to tether to the ODN. Thus, we have compared the stabilities and the binding geometries of tethered $[Ru(phen)_2dppz]^{2+}$ in the duplexes formed with **10**, **11**, or **12** with the target ODN **9** and compared them with the dppz-tethered counterparts (as in **10′**, **11′**, and **12′**).[21] We here show that the change of the ODN-spacer attachment site in the tethered $[Ru(phen)_2dppz]^{2+}$ complex from phen to the dppz moiety indeed plays an important role in the recognition of the tethered Ru^{2+} complex by the DNA double helix in that we observe a dramatic T_m rise of the DNA·DNA duplexes, with ΔT_m varying from 13 to 23 °C, depending upon whether the Ru^{2+} complex was tethered at the 3′-, in the middle, or at the 5′-end of the 9mer **9**.

The $[Ru(phen)_2dppz]^{2+}$-labeled ODNs have been prepared using the phosphoramidite chemistry.[17] The $[Ru(phen)_2dppz]^{2+}$ derivatized building block **5** was constructed such that it could be introduced at the 3′-, 5′-, or at the interior of the 9mer ODN strand by choice, basing on a non-nucleosidic *sn*-glycerol-tri(ethylene glycol) fused linker. The comparison of the CD data of the single-stranded Ru^{2+}-ODN and the double-stranded (Ru^{2+}-ODN)·DNA duplex, along with the comparison of T_m and $\Delta G°$ and the results of digestion by DNase I of the latter showed the extent and location of structural distortions caused by interaction of Ru^{2+} complex within the DNA duplex framework.

Results and Discussion

(I) Synthesis of Ru^{2+}-Labeled Oligodeoxyribonucleotides. Preparation of the synthetic ODNs with tethered metal complex by standard solid-state synthesis required the development of a bifunctional linker in which one of the functional groups can be protected while the other is activated. We chose *sn*-glycerol-tri(ethylene glycol) fused linker[21−23] for this purpose because of its hydrophilic and flexible character, permitting the incorporation of the metal complex either between the two phosphodiester residues of the ODN or into the 3′- or 5′-terminal of the ODN chain.

The $[Ru(phen)_2dppz]^{2+}$ derivatized building block **5** was synthesized as follows in five steps, $\mathbf{1}^{24} \rightarrow \mathbf{2}^{18} \rightarrow \mathbf{3}^{18} \rightarrow \mathbf{5}$ (Figure 1): The precursor acidic complex **3** was previously obtained[18] in two steps starting from $Ru(phen)_2Cl_2$ **1** which was complexed with 1,10-phenanthroline-5,6-dione[17] to give the racemic (Δ/Λ) $[Ru(phen)_2(phendione)](PF_6)_2$ **2**. It was then condensed with 3,4-diaminobenzoic acid to give the desired -COOH group in $[Ru(phen)_2(dppz\text{-}COOH)](PF_6)_2$ **3** (dppz-COOH = dipyridophenazine-11-carboxylic acid) in a straightforward manner. Activation of the racemic mixture of Δ- and Λ-enantiomeric carboxylic acids **3** with 1,1′-carbonylbis[1*H*-imidazole] and the treatment of intermediate complex with *sn*-glycerol derivatized amine **4**[21] in pyridine at room temperature gave the key amide **5** (59%). It is important to note that using racemic (Δ/Λ)-mixture of metallocomplex **3** and (*R*/*S* from *sn*-glycerol)-mixture of the linker **4** gives four possible isomers of compound **5** (Δ_R, Δ_S, Λ_R, and Λ_S) [(Δ_R/Λ_S) and (Δ_S/Λ_R) are two pairs of enantiomers]. As a consequence, all subsequent derivatives of compound **5** (including the ODN conjugates) described in this paper should exist in four isomeric forms. Complex **5** as well as the precursors **2** and **3** were isolated as the PF_6^- salts, which ensured their solubility in organic solvents for subsequent use in the automated DNA/RNA synthesizer. In the final step, the compound **5** was converted in the usual manner[25] to the corresponding phosphoramidite block **6** (94%) for incorporation of the $[Ru(phen)_2dppz]^{2+}$-derivatized monomer unit into the 5′-end or in the middle of an ODN. Compound **5** was also treated with succinic anhydride and DMAP in CH_2Cl_2 to give the corresponding succinate block **7** (86%) which was then immobilized onto aminopropyl-CPG support[26] and was used for incorporation of the $[Ru(phen)_2dppz]^{2+}$-tethered building block at the 3′-terminus of the ODN.

In this study, we prepared three $[Ru(phen)_2dppz]^{2+}$-tethered ODNs **10**−**12** (Table 1) by the phosphoramidite methodology[27] on a commercially available DNA/RNA synthesizer. The model nucleotide sequence chosen in the above oligos was identical to the dppz-ODN conjugates used in our previous study,[21] thereby allowing us to compare the present data with those published. Removal of the finished 9mer ODNs from the solid support using concentrated ammonium hydroxide was followed by incubation at 55 °C for 17 h to afford the deprotected ODNs

(13) Hurley, D. J.; Tor, Y. *J. Am. Chem. Soc.* **1998**, *120*, 2194−2195.
(14) Khan, S. I.; Beilstain, A. E.; Grinstaff, M. W. *Inorg. Chem.* **1999**, *38*, 418−419.
(15) Bannwarth, W.; Schmidt, D. *Tetrahedron Lett.* **1989**, *30*, 1513−1516.
(16) Khan, S. I.; Beilstain, A. E.; Sykora, M.; Smith, G. D.; Hu, X.; Grinstaff, M. W. *Inorg. Chem.* **1999**, *38*, 3922−3925.
(17) Hiort, C.; Linkoln, P.; Norden, B. *J. Am. Chem. Soc.* **1993**, *115*, 3448−3454.
(18) Hartshorn, R. M.; Barton, J. K. *J. Am. Chem. Soc.* **1992**, *114*, 5919−5925.
(19) Murphy, C. J.; Arkin, M. R.; Jenkins, Y.; Ghatlia, N. D.; Bossmann, S. H.; Turro, N. J.; Barton, J. K. *Science* **1993**, *262*, 1025−1029.
(20) Moucheron, S.; Kirsch-De Mesmaeker, A.; Kelly, J. M. *J. Photochem. Photobiol., B* **1997**, *40*, 91−106.
(21) Ossipov, D.; Zamaratski, E.; Chattopadhyaya, J. *Helv. Chim. Acta* **1999**, *82*, 2186−2200.
(22) Willis, M. C.; Collins, B.; Zhang, T.; Green, L. S.; Sebesta, D. P.; Bell, C.; Kellogg, E.; Gill, S. C.; Magallanez, A.; Knauer, S.; Bendele, R. A.; Gill, P. S.; Janjic, N. *Bioconjugate Chem.* **1998**, *9*, 573−582.
(23) Timofeev, E. N.; Smirnov, I. P.; Haff, L. A.; Tishchenco, E. I.; Mirzabekov, A. D.; Florentiev, V. L. *Tetrahedron Lett.* **1996**, *47*, 8467−8470.
(24) Sullivan, B. P.; Salmon, D. J.; Meyer, T. J. *Inorg. Chem.* **1978**, *17*, 3334−3341.
(25) Sinha, N.; Biernat, J.; Köster, H. *Tetrahedron Lett.* **1983**, *24*, 5843−5846.
(26) *Oligonucleotide Synthesis. A Practical Approach*; Gait, M. J., Ed.; IRL Press: Oxford. 1984; p 45.
(27) Matteucci, M. D.; Caruthers, M. H. *J. Am. Chem. Soc.* **1981**, *103*, 3185−3191.

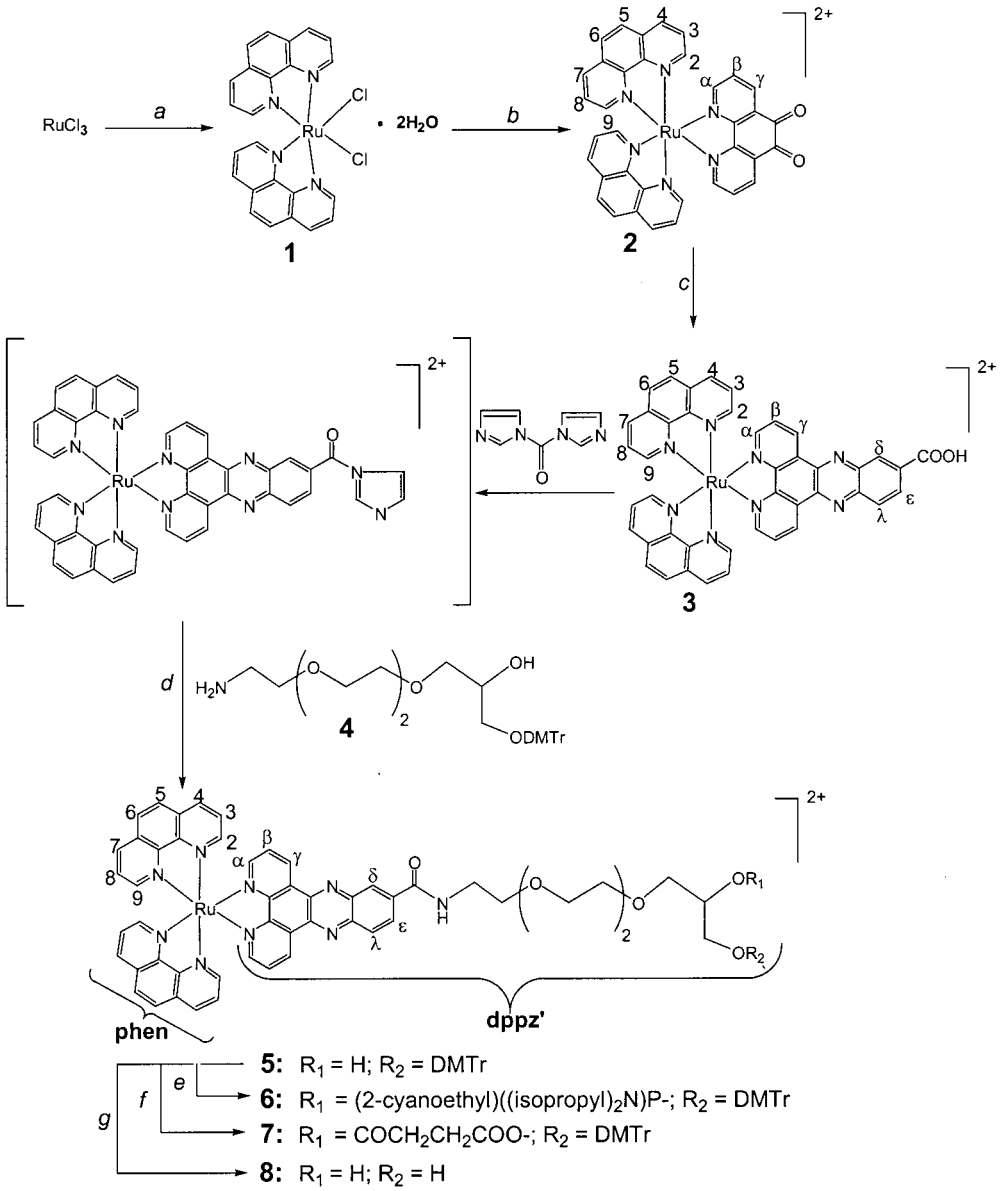

Figure 1. (a) 1,10-phenantroline, LiCl, DMF, 8 h, reflux; (b) 1,10-phenantroline-5,6-dione, ethanol:water 1:1, 4 h, reflux; (c) 3,4-diaminobenzoic acid, ethanol, 15 min, reflux; (d) *N*,*N*′-carbonyldiimidazole, pyridine, 0.5 h, 20 °C; **4**, 2.5 h, 20 °C; (e) (2-CeO)-((ipr)$_2$N)-PCl, (ipr)$_2$EtN, THF, 1.5 h, 20 °C; (f) succinic anhydride, DMAP, CH_2Cl_2, 4 h, 20 °C; (g) acetic acid, 10 min, 20 °C.

10−**12** which were purified by reverse-phase HPLC with a gradient of 5−50% CH_3CN containing 0.1 M triethylammonium acetate, pH 7.0.

The HPLC separation (Figure 2A) of the middle Ru^{2+}-labeled ODN **12** gave well-resolved two pure Λ-isomers (*R* and *S*) **12a**, **12b**, and two pure Δ-isomers (*R* and *S*) **12c**, **12d**, according to the CD analysis (see below) (*R* and *S* cannot however be assigned for **12a**−**d**). The 5′-Ru^{2+}-modified ODN **10** could only be resolved into two fractions (Figure 2B). The 3′-Ru^{2+}-modified oligo **11,** exhibited an unresolved single peak, despite our attempts to separate them with various eluents and gradient systems. Satisfactory separation of the constituent stereoisomers of the middle Ru^{2+}-labeled ODNs **12a**−**d** might be a consequence of different chemospecific interactions of the Ru^{2+} ligands (Δ and Λ) with the chiral environment of the single-stranded ODN. Analytical gel electrophoresis of the purified diastereomers of the middle Ru^{2+}-modified ODN **12a**−**d** is shown in Figure 3.

The ODN-conjugates synthesized have been characterized by matrix-assisted laser desorption ionization time-of-flight mass spectrometry (MALDI-TOF-MS). The calculated mass for all conjugates is 3720.8 ($C_{139}H_{154}N_{42}O_{58}P_9Ru$ including ^{102}Ru isotope), and the observed *m*/*z* was respectively found at 3720.6 for oligo **10**, 3720.4 for **11**, 3720.8 for **12b**, and 3720.3 for a **12c**/**12d** mixture. From these data one can conclude all substances are indeed the desired conjugates. Further structural evidence showing the correct incorporation site of the [Ru(phen)$_2$dppz]$^{2+}$ moiety at the middle of ODN (i.e., between ^{4}**A** and ^{5}**A**, see Figure 8A for numbering) came from the partial digestion of **12a**−**d** with snake venom phosphodiesterase (SVP), a 3′-exonuclease, and spleen phosphodiesterase, a 5′-exonuclease, followed by MALDI-TOF MS of the digest. The MS measurement after 5 min of SVP degradation in pure water showed a mixture consisting of the molecular ion at *m*/*z* 3722.17, and products corresponding to loss of ^{9}**T** residue at *m*/*z* = 3417.97, followed by loss of ^{8}**A** residue (*m*/*z* = 3104.7), ^{7}**C** residue (*m*/*z* = 2815.45), and ^{6}**A** residue (*m*/*z* = 2502.2). Then the digestion stops at ^{5}**A**. A similar partial digestion study by the spleen phosphodiesterase for 5 min, followed by MALDI-TOF showed no molecular ion at *m*/*z* 3722.17, but the products

Table 1. Synthetic Ru^{2+}-Labeled ODN Conjugates (Modification Is Designated as **X**) and Their Target Oligo-DNA and Oligo-RNA[a]

	oligos		compd
	natural	5′-d(TCCAAACAT)	**9**
9mers	5′-modified	5′-d(**X**TCCAAACAT)	**10**
		5′-d(**Y**TCCAAACAT)	**10′**
	3′-modified	5′-d(TCCAAACAT**X**)	**11**
		5′-d(TCCAAACAT**Y**)	**11′**
	middle	5′-d(TCCA**X**AACAT)	**12**
		5′-d(TCCA**Y**AACAT)	**12′**
11mers	single strand	5′-d(CATGTTTGGAC)	**13**
	targets	5′-r(CAUGUUUGGAC)	**14**

[a] For comparison the dppz-tethered ODNs (modification is designated as **Y**) are entered

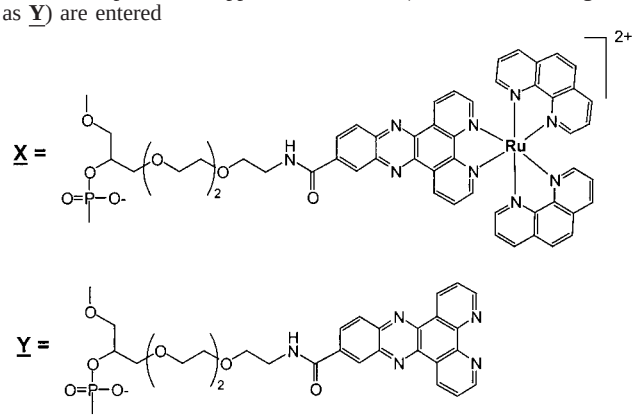

from the digestion consisted of a peak at $m/z = 3419.6$ owing to the loss of **[1]T** residue and a peak at $m/z = 3130.3$ due to the loss of **[2]C** residue, and then the digestion stopped finally at **[4]A** residue after the loss of **[3]C** ($m/z = 2840.8$). These partial exonuclease digestion studies both from the 3′- and 5′-ends showed that **[4]A** and **[5]A** residues are resistant to both exonucleases, which supports that the tethered $[Ru(phen)_2dppz]^{2+}$ moiety have been indeed introduced between the **[4]A** and **[5]A** residues.

(II) CD Spectroscopy of Ru^{2+}-labeled ODNs and the (Ru^{2+}-ODN)·DNA Duplexes. As it has been mentioned above, the preparative HPLC chromatogram of the middle-modified 9mer ODN consisted of four product peaks of nearly equal intensity (Figure 2A), which were collected separately in ascending order of their retention times (**12a**, **12b, 12c**, and **12d**). The electrophoretic mobilities of these fractions were the same (Figure 3), while their CD spectra (Figure 4A) argued that they belong to different isomers of the middle Ru^{2+}-labeled 9mer ODN. Comparison of our CD spectra with those of the literature data for free $[Ru(phen)_2dppz]^{2+}$ complex[28,29] or tethered to the 5′-termini of ODN[12] has led us to assign **12a** and **12b** with the tethered Ru^{2+} complex in two possible Λ-configurations (*S* and *R*), and assign **12c** and **12d** in the two mirrored Δ-configurations. On the basis of equal and opposite relationship of the CD spectra as well as equal intensity of all four HPLC peaks (Figure 2A), one can conclude that none of the diastereomers was formed preferentially. In contradistinction, the CD spectra of two fractions obtained in the course of HPLC purification of 5′-Ru^{2+}-ODN **10** (Figure 2B) showed the corresponding bands of opposite signs but different intensity (Figure 4B), which did not allow us to clearly assign the distribution of four diastereomers in the two fractions **10a** and **10b**.

(28) Eriksson, M.; Leijon, M.; Hiort, C.; Norden, B.; Gräslund, A. *Biochemistry* **1994**, *33*, 5031−5040.
(29) Franklin, S. J.; Treadway, C. R.; Barton, J. K. *Inorg. Chem.* **1998**, *37*, 5198−5210.

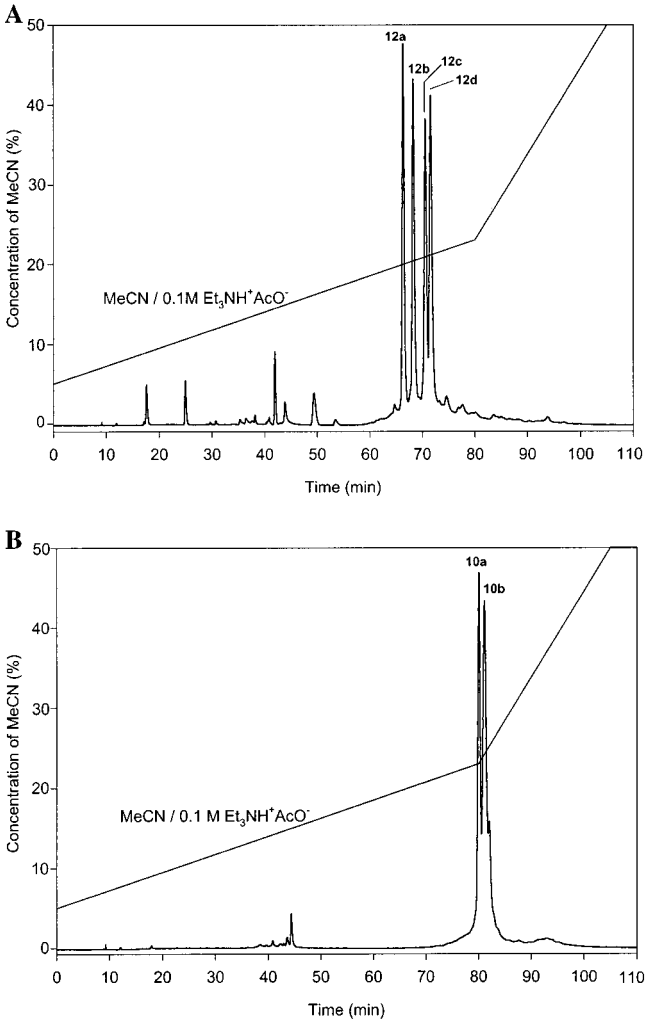

Figure 2. (A) Reversed-phase HPLC of the crude mixture of Ru^{2+} middle-modified ODN **12**. (B) Reversed-phase HPLC of the crude mixture of 5′-Ru^{2+} modified ODN **10**.

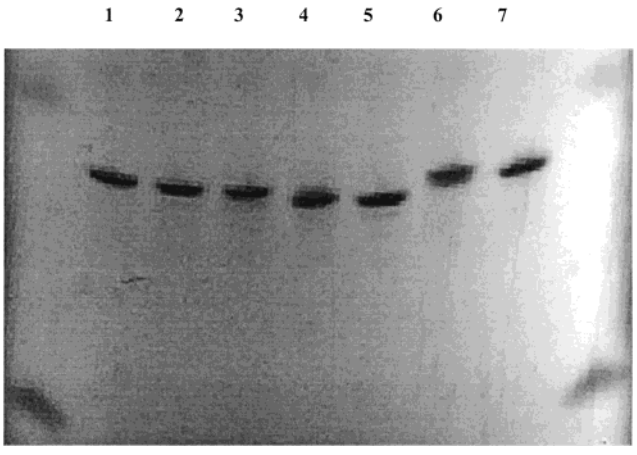

Figure 3. UV-shadowing PAGE ($\lambda = 254$ nm) of Ru^{2+}-labeled ODNs: **11** (lane 1), **12d** (lane 2), **12c** (lane 3), **12b** (lane 4), **12a** (lane 5), **10b** (lane 6), **10a** (lane 7) showing their purities.

The CD spectra of the racemic Ru^{2+}-ODN conjugates hybridized with the DNA target **13** were recorded to exclude the contribution of the CD signal originated from each of the pure Ru^{2+} complex diastereomer in order to observe the global helical conformation of the DNA duplex framework (Figure 5). The CD spectra of the natural duplex **9·13** was used for comparison. It can be seen that for 5′- and middle-modified

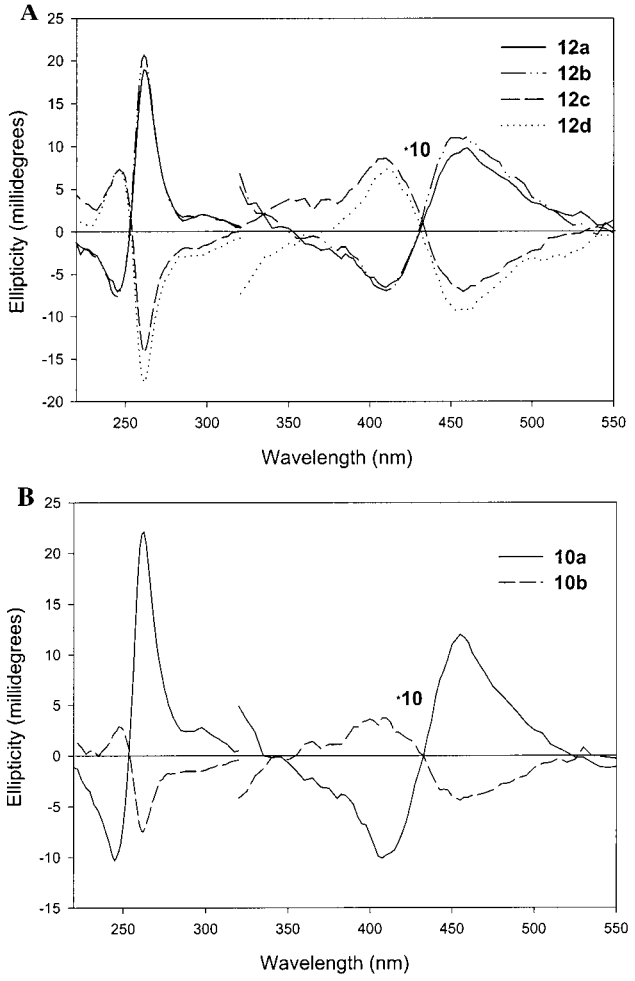

Figure 4. (A) CD spectra of diastereomers of Ru^{2+} middle-modified ODN **12**. (B) CD spectra of fractions **10a** and **10b** of 5′-Ru^{2+}-modified ODN.

duplexes **10·13** and **12·13** the positive band is centered near $\lambda = 260$ nm and the negative band centered near $\lambda = 232.5$ nm which is shifted by 7.5 nm from the corresponding native maximum (267.5 nm) and minimum (240 nm) to the short wave area. The CD crossover of 5′- and the middle-modified duplexes **10·13** and **12·13** is centered near $\lambda = 246.3$ nm which is shifted by 5 nm from the native counterpart (251.3 nm) to the short wave area. The CD spectra of 3′-modified duplex **11·13** exhibits features which is characteristic for the natural duplex: i.e. the same negative band minimum (240 nm) and a shoulder at 267.5 nm which coincides with the native duplex positive band. It also shows the same crossover point (246.3 nm) and shifted main positive band as in the 5′- and middle modified duplexes **10·13** and **12·13**. These features suggest that the gobal conformation of **10·13** and **12·13** are different from **11·13**. They altogether differ from the B-form of DNA,[30] and have features that are reminiscent of the A-type helix.[31]

The structural changes in the enantiomerically pure Ru^{2+}-ODN conjugates (**12a**−**d**) upon its hybridization with the DNA target have also been explored. The CD spectra of (Ru^{2+}-ODN)·DNA duplexes **12a·13**, **12b·13**, **12c·13**, and **12d·13** (Figure 6) were compared to the CD spectra of enantiomerically pure single-stranded Ru^{2+}-ODNs recorded at 5 °C: For the middle-modified Δ-isomers **12c** and **12d** the intensity of the short (246 nm) wavelength band essentially increases upon hybridization, while the corresponding band for the Λ-isomers duplexes **12a·13** and **12b·13** increases very little. Additionally, the long wavelength band at 262 nm is notably broadened upon hybridization of the Δ-isomers **12c** and **12d** in contrast with the Λ-isomers **12a·13** and **12b·13**, which exhibit sharp 262 nm band in the duplex form. Taken together, these facts denote somewhat different binding geometries for Δ- and Λ-diastereoisomers of the Ru^{2+} complex tethered at the middle of the 9mer DNA in the duplex form compared to the single-stranded counterpart, which is also evident from their relative thermodynamic stabilities as well as recognition and cleavage by DNase I (see below).

(III) Thermal Melting Study of Intermolecular Ru^{2+} Complexes and DNA·DNA Duplex. Prior to the melting of (Ru^{2+}-ODN)·DNA and (Ru^{2+}-ODN)·RNA hybrids, we have examined the influence of some nonconjugated ruthenium complexes on the stability of natural DNA·DNA duplex **9·13** (ruthenium complex (1−5 μM) added to the native duplex **9·13** (1 μM) in 20 mM PO_4^{3-}, 0.1 M NaCl buffer at pH 7.3). In this study, $[Ru(phen)_2dppz](PF_6)_2$ and $[Ru(phen)_3](PF_6)_2$ were compared to the $[Ru(phen)_2(dppz\text{-}CONH(CH_2CH_2O)_3CH_2CH(OH)CH_2OH)](PF_6)_2$ **8**, to examine the effect of the linker in the Ru^{2+}-labeled ODNs **10**−**12**. It has been earlier shown that most polypyridyl Ru^{2+} complexes are positively charged, and may thus bind electrostatically to the single- or double-stranded (ds) DNA at low ionic strength.[32,33] In dsDNA, they may also undergo partial intercalation between two DNA base pairs,[33−35] when one of the ligands is an extended polyazaaromatic planar system. Another feasible binding mode of such complexes with dsDNA is a groove-bound interaction.[36] Various methods, including fluorescence quenching,[37] flow linear dichroism,[17] NMR spectroscopy,[38] and topoisomerase unwinding assay[37,39] have confirmed that $[Ru(phen)_2dppz](PF_6)_2$ is a typical metallointercalator, while for $[Ru(phen)_3](PF_6)_2$ both intercalative and surface binding modes can be accepted.

It can be seen from Figure 7 that two types of behavior are observed for the complexes selected: For $[Ru(phen)_2dppz](PF_6)_2$ and the new complex **8**, T_m increases sharply with an increase of the amount of the complex added to the DNA·DNA duplex **9·13**. In this case temperature curves have strongly marked kink points ([ruthenium]/[DNA phosphate] or D/P = 0.15−0.2; i.e. 3−4 equiv of ruthenium complex per 9mer + 11mer duplex **9·13**), after which T_m increase becomes slow. On the other hand, growing amount of $[Ru(phen)_3](PF_6)_2$ does not practically result in the duplex stabilization. This observation is in agreement with the earlier study on some polypyridyl Ru^{2+} complexes as DNA binders.[40] Since the plot of T_m versus D/P for $[Ru(phen)_2dppz](PF_6)_2$ and the new complex **8** are very similar and since the former stabilizes DNA duplex by intercalating with the dppz moiety, we conclude that our complex **8** intercalates in a very

(30) Allen, F. S.; Gray, D. M.; Roberts, G. P.; Tinoco, I. *Biopolymers* **1972**, *11*, 853−879.
(31) Fasman, G. *Handbook of Biochemistry and Molecular Biology*; CRC Press: Ohio, 1975; Vol 1, p 589.
(32) Hiort, C.; Norden, B.; Rodger, A. *J. Am. Chem. Soc.* **1990**, *112*, 1971−1982.
(33) Kelly, J. M.; Tossi, A. B.; McConnel, D. J.; OhUigin, C. *Nucleic Acids Res.* **1985**, *13*, 6017−6034.
(34) Barton, J. K. *J. Biomol. Struct. Dyn.* **1983**, *1*, 621−632.
(35) Long, E. C.; Barton, J. K. *Acc. Chem. Res.* **1990**, *13*, 271−273.
(36) Rehmann, J.; Barton, J. K. *Biochemistry.* **1990**, *29*, 1701−1710.
(37) Friedman, A. E.; Chambron, J. C.; Sauvage, J. P.; Turro, N. J.; Barton, J. K. *J. Am. Chem. Soc.* **1990**, *112*, 4960−4962.
(38) Dupureur, C. M.; Barton, J. K. *J. Am. Chem. Soc.* **1994**, *116*, 10286−10287.
(39) Jenkins, Y.; Friedman, A. E.; Turro, N. J.; Barton, J. K. *Biochemistry* **1992**, *31*, 10809.
(40) Tossi, A. B.; Kelly, J. M. *J. Photochem. Photobiol.* **1989**, *49*, 545−556.

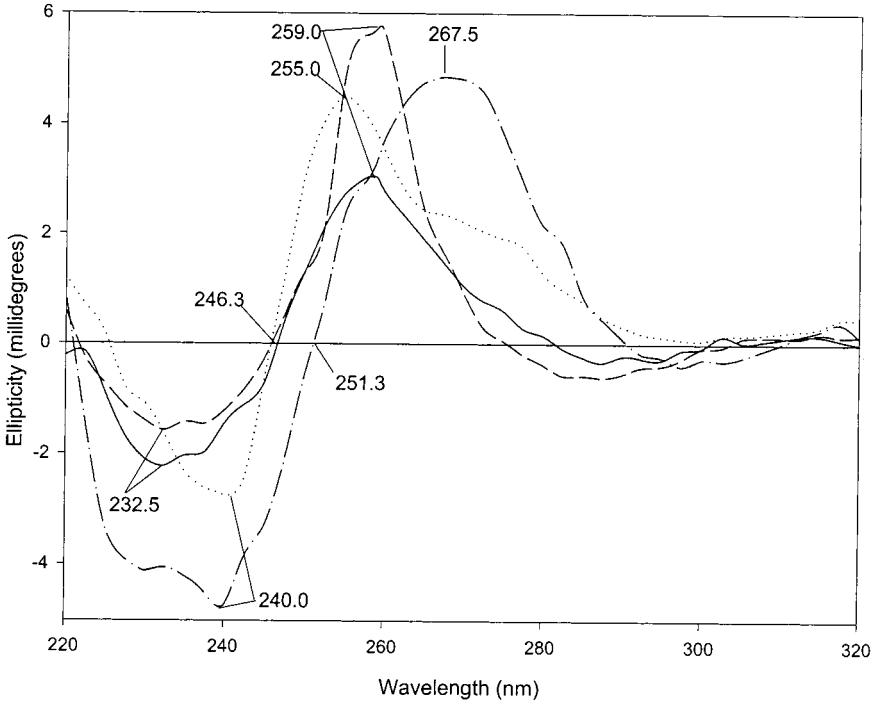

Figure 5. CD spectra of racemic (Ru^{2+}-DNA)·DNA duplexes as a function of wavelength (nm): **10·13** (—), **11·13** (···), **12·13** (− − −). CD spectra of nonmodified DNA·DNA duplex **9·13** (− · −) is shown for comparison.

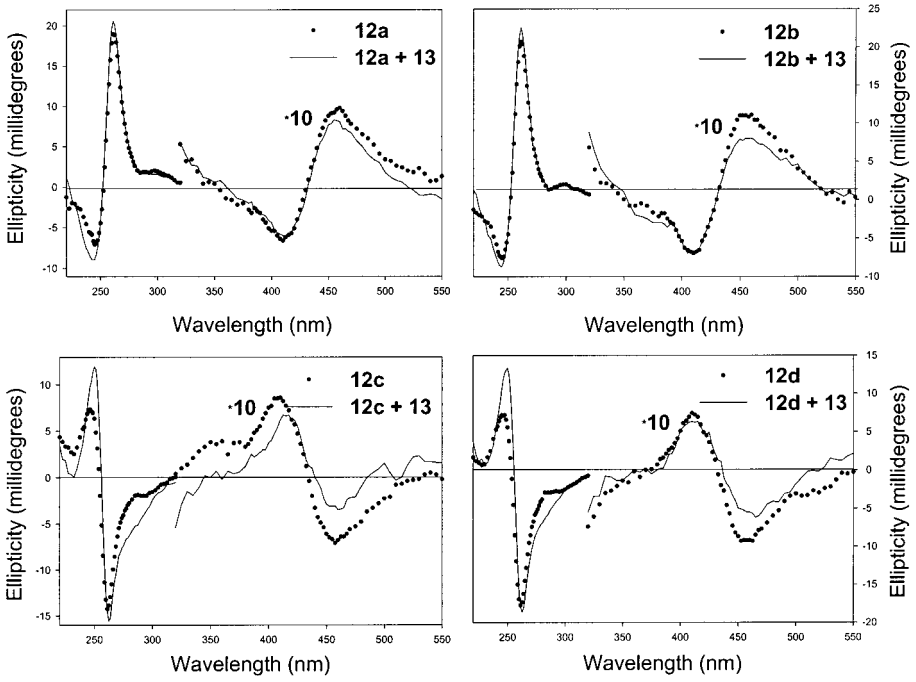

Figure 6. CD spectra of diastereomers of Ru^{2+} middle-modified ODN **12** (dotted curves) and their corresponding duplex spectra (full curves).

similar way, despite the fact that the dppz ligand in the latter is sterically hindered by covalent attachment of the linker arm. This assumption can be supported by the fact that $[Ru(phen)_3](PF_6)_2$, which interacts with DNA by only its phenanthroline ligands, showed very small stabilization and shallow T_m rises with D/P.

Another factor which demonstrated intercalative character for both $[Ru(phen)_2dppz](PF_6)_2$ and the complex **8** was the thermal denaturation curve width (S_t) when they were mixed with DNA·DNA duplex **9·13**. The temperature range within which 10−90% of duplex denaturation occurs is 25−25.5 °C, whereas for the mixture of $[Ru(phen)_3](PF_6)_2$ and **9·13**, it is only 17.5 °C. Large S_t value is responsible for intercalation at low intercalator concentration because the stabilization near the binding sites is greater than for the base pairs distant from the bound complexes.[35]

(IV) Thermal Melting Study of (Ru^{2+}-ODN)·DNA Duplexes. The (Ru^{2+}-ODN)·DNA duplexes (entries 2−8 in Table 2) were generated by hybridization of the Ru^{2+}-ODNs **10**−**12** with the target 11mer ODN **13** in a 1:1 ratio (1 μM of each strand in 20 mM PO_4^{3-}, 0.1 M NaCl buffer at pH 7.3). All of the melting curves of these duplexes showed a monophasic dissociation, and Table 2 shows the melting temperatures, which leads to the following conclusions: *Tethering the [Ru(phen)$_2$dppz](PF$_6$)$_2$ through the dppz moiety at all positions of the 9mer strand (3′- or 5′-termini or at the middle) leads to the dramatic*

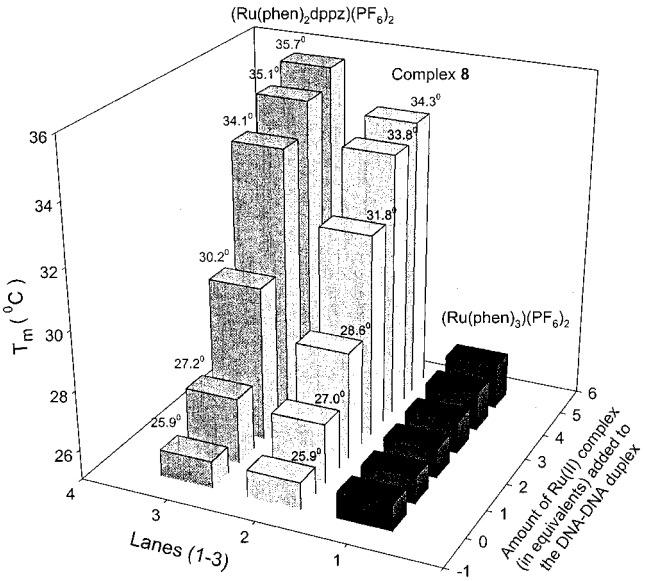

Figure 7. Plots for the melting temperature (T_m) vs metal complex concentration, for DNA·DNA duplex **9·13** in the presence of: [Ru(phen)$_3$](PF$_6$)$_2$ (lane 1), [Ru(phen)$_2$dppz](PF$_6$)$_2$ (lane 3) and complex **8** (lane 2). The T_m was calculated from denaturation curves of duplex **9·13** (1 μM) in buffer I (see Experimental Section).

Table 2. Thermal Stability (T_m in °C) of (Ru^{2+}-DNA)·DNA and (Ru^{2+}-DNA)·RNA Duplexes[a] (1:1 mixture)

DNA·DNA duplexes				DNA·RNA duplexes			
entries	duplex-type[a]	T_m	ΔT_m	entries	duplex-type[a]	T_m	ΔT_m
1	**9·13**	25.4	−	9	**9·14**	20.6	−
2	**10a·13**	48.8	23.4	10	**10·14**	29.7	9.1
3	**10b·13**	47.0	21.6				
3	**11·13**	38.2	12.8	11	**11·14**	28.5	7.9
5	**12a·13**	41.8	16.4	12	**12a·14**	20.6	0.0
6	**12b·13**	44.8	19.4	13	**12b·14**	21.6	1.0
7	**12c·13**	39.0	13.6	14	**12c/d·14**	20.1	−0.5
8	**12d·13**	39.7	14.3				

[a] Oligos **10** and **11** are the mixtures of ODNs attached to the Ru^{2+} complex in all possible configurations (Δ_R, Δ_S, Λ_R, Λ_S). **10b** = **10** − **10a**.

Table 3. Thermal Stability (T_m in °C) of (dppz-DNA)·DNA and (dppz-DNA)·RNA Duplexes (1:1 mixture)[21]

DNA·DNA duplexes				DNA·RNA duplexes			
entries	duplex-type[#]	T_m	ΔT_m	entries	duplex-type[#]	T_m	ΔT_m
1	**9·13**	25.4	−	5	**9·14**	20.6	−
2	**10′·13**	37.4	12.0	6	**10′·14**	26.1	5.4
3	**11′·13**	36.3	10.9	7	**11′·14**	25.2	4.5
4	**12′·13**	30.4	5.0	8	**12′·14**	21.5	0.9

increase of the corresponding 9mer + 11mer DNA·DNA duplex stability (ΔT_m fluctuates from 12.8 to 23.4 °C). To our knowledge, this is the first example of such a large DNA·DNA duplex stabilization achieved so far by covalent linking of Ru^{2+} complexes. It is noteworthy that the best stabilization achieved before this work was 3 °C[6a] and 8 °C[8] for 5′-tethered [Ru(phen)$_2$dppz](PF$_6$)$_2$ when the phen ligand was used for covalent attachment, while for duplexes with other types of Ru^{2+}-ODN complexes[7,9,10,12] no improvement in the stabilization has been observed.

Simple inspection of Tables 2 and 3 shows (compare with the corresponding dppz[17] and the native counterparts) that the most preferable form of conjugation is through the 5′-tether as in **10a·13** (ΔT_m = 23.4 °C). The middle tethered Ru^{2+} conjugate, as in **12b·13**, results also in very high duplex stabilization (ΔT_m = 19.4 °C). It should be noted that absolute ligand configuration at the Ru^{2+} center of the complex plays an essential role for the DNA hybridization. For the enantiomerically pure middle modified ODNs, for example, one can see that Λ-Ru^{2+} complex gives higher stabilization (ΔT_m = 19.4 °C and 16.4 °C for two possible orientation of the tri(ethylene glycol) spacer at the tertiary *sn*-glycerol carbon). On the other hand, the corresponding Δ-Ru^{2+} complex gives relatively poorer stabilization (ΔT_m = 14.3 and 13.6 °C). The same tendency is observed for the 5′-(Ru^{2+}-ODN)·DNA duplexes: **10a·13** is more stable (ΔT_m = 23.4 °C) than **10b·13** (ΔT_m = 21.6 °C). Finally, 3′-Ru^{2+}-conjugation gives the least stabilization (ΔT_m = 12.8 °C). Thus the strength of duplex stabilization for various site-specific Ru^{2+} incorporations into ODN are as follows: 5′-Ru^{2+}→ middle Ru^{2+}→ 3′-Ru^{2+}-modified duplex.

Table 4. Thermodynamic Parameters for DNA·DNA Duplex Formation

duplex	T_m °C	ΔT_m °C	$\Delta H°$ kJ mol^{-1}	$\Delta S°$ kJK^{-1}mol^{-1}	$T_{298}\Delta S°$ kJ mol^{-1}	$\Delta G°$ kJmol^{-1}
9·13	25.4	−	−240.4 ± 20.4	−0.68 ± 0.06	202.6	−37.8
10′·13	37.4	12.0	−252.7 ± 8.2	−0.69 ± 0.03	205.6	−47.1
11′·13	36.3	10.9	−275.5 ± 7.4	−0.77 ± 0.02	229.5	−46.0
12′·13	30.4	5.0	−243.3 ± 17.4	−0.68 ± 0.06	202.6	−40.7
10a·13	48.8	23.4	−254.6 ± 15.5	−0.67 ± 0.05	199.7	−54.9
10b·13	47.0	21.6	−230.4 ± 17.2	−0.60 ± 0.05	178.8	−51.6
11·13	38.2	12.8	−279.5 ± 15.9	−0.78 ± 0.05	232.4	−47.1
12a·13	41.8	16.4	−263.2 ± 20.9	−0.72 ± 0.06	214.6	−48.6
12b·13	44.8	19.4	−228.0 ± 15.6	−0.60 ± 0.05	178.8	−49.2
12c·13	39.0	13.6	−243.9 ± 20.3	−0.66 ± 0.06	196.7	−47.2
12d·13	39.7	14.3	−268.0 ± 22.6	−0.74 ± 0.07	220.5	−47.5

(V) Thermodynamics of DNA·DNA Duplex Formation. Melting curves with a series of DNA concentrations (2, 4, 6, 8, and 10 μM of total strand concentration) were recorded for (Ru^{2+}-ODN)·DNA duplexes including natural duplex and dppz-conjugated analogues for comparison. Thermodynamic parameters were calculated according to an "all-or none" two-state model, and are listed in Table 4. As seen from this Table, the introduction of a Ru^{2+} complex in a duplex gives a more negative $\Delta G°$ (i.e., stabilization increases by 9.3−17.1 kJ/mol) compared to the unmodified counterpart ($\Delta G°$ = −37.8 kJ/mol), which is in accordance with the enhanced thermal stability of ruthenated duplexes. There is also a correlation between the difference in the free energy ($\Delta\Delta G°$) and the change of melting temperature (ΔT_m): 5′-(Ru^{2+}-ODN)·DNA (ΔT_m = 23.4−21.6 °C, $\Delta\Delta G°$ = −17.1/−13.8 kJ/mol) > middle-(Ru^{2+}-ODN)·DNA (ΔT_m = 19.4−13.6 °C, $\Delta\Delta G°$ = −11.4/−9.4 kJ/mol) > 3′-(Ru^{2+}-ODN)·DNA (ΔT_m = 12.8 °C, $\Delta\Delta G°$ = −9.3 kJ/mol) > natural duplexes.

Differences found in the thermodynamic data for the most of the Ru^{2+}-modified DNA−DNA duplexes and the natural counterpart are of the same order of magnitude as their calculated errors (±3−9%). This simply did not allow us to identify a clear trend of competing enthalpy and entropy contribution in the observed $\Delta G°$ of stabilization of the duplexes, in general.

(VI) Mechanism of the Stabilization of (Ru^{2+}-ODN)·DNA Duplexes. The high stability observed for (Ru^{2+}-ODN)·DNA duplexes is presumably owing to the intercalation of the dppz subunit between stacked base pairs in a very similar way found for bis-ruthenium complex.[41] This intercalative interaction is energetically optimal because of the large π-stacking area available for the dppz moiety (distance between Ru^{2+} and ϵ-C of dppz is 9.93 Å, Figure 1) with the adjacent base pairs (the distance across two distal atoms of a base pair is being ∼9.9

(41) Önfelt, B.; Lincoln, P.; Norden, B. *J. Am. Chem. Soc.* **1999**, *121*, 10846−10847.

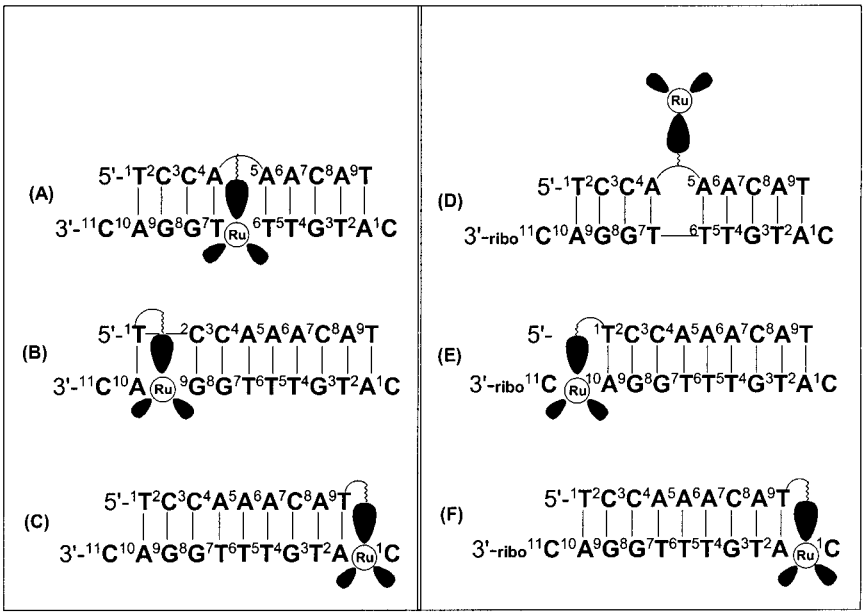

Figure 8. Schematic illustration of the positioning of the metal complex in the differently Ru^{2+}-labeled DNA·DNA duplexes (A−C) and DNA·RNA duplexes (D−F).

Å), which clearly is not possible for the phen group to cover (4.77 Å being the distance between two distal atoms). For our tethered $[Ru(phen)_2dppz]^{2+}$-ODN, the dppz intercalation can be realized if the $Ru(phen)_2$ moiety passes through the DNA strands to reach their final position, or the linker has to sling itself around the opened base pairs. This threading through DNA should produce a very rigid structure in which covalently attached complex acts as a staple,[41] holding the DNA·DNA duplex bases tightly stacked together near the intercalation site promoting a conformational reorganization with a net free-energy gain, which is also consistent with the CD properties.

With the above scenario, the decrease of DNA·DNA duplex stability from 5′ > middle > 3′-modified duplex can be explained by the following model: For the most stabilized 5′-modified duplex **10·13** and middle-modified duplex **12·13** the tethered $[Ru(phen)_2dppz]^{2+}$ complex threads through the duplex core ensuring the dppz intercalation between two base pairs. The bulged abasic site between **^{4}A·^{7}T** and **^{5}A·^{6}T** doublets as well as neighboring sites are accessible for such threading in the middle-modified duplex **12·13** (Figure 8A), while in 5′-modified duplex **10·13** the dppz ligand intercalates between **^{1}T·^{10}A** and **^{2}C·^{9}G** or perhaps between **^{2}C·^{9}G** and **^{3}C·^{8}G** base pairs (Figure 8B). In the 3′-modified duplex **11·13** the metallo-intercalator covers only terminal base pair **^{9}T·^{2}A** (Figure 8C) which should be less effective in terms of net stabilization of the duplex.

(VII) Thermal Melting Study of (Ru^{2+}-ODN)·RNA Duplexes. The hybrid duplexes (Ru^{2+}-ODN)·RNA (entries 10−14 in Table 2) were generated by hybridization of the Ru^{2+}-tethered 9mers **10**−**12** with the target 11mer RNA **14** in a 1:1 ratio (1 μM of each strand in 20 mM PO_4^{3-}, 0.1 M NaCl buffer at pH 7.3). Thermal denaturation study on the internally modified (Ru^{2+}-ODN)·RNA duplexes showed no stabilization for any of the diastereoisomers (entries 12−14 in Table 2) in contrast with the (Ru^{2+}-ODN)·DNA counterpart. The 5′- and 3′-conjugated (Ru^{2+}-ODN)·RNA duplexes **10·14** and **11·14** are, however, found to be more stable than the natural counterpart (ΔT_m = 9.1 °C and 7.9 °C respectively, entries 10−11 in Table 2). It is likely that the 5′- and 3′-conjugated (Ru^{2+}-ODN)·RNA duplexes are stabilized in a manner similar to that of the corresponding (3′-Ru^{2+}-ODN)·DNA duplexes (compare Figure 8C with 8E and 8F). On the other hand, the reason for lack of stabilization of the middle-modified (Ru^{2+}-ODN)·RNA duplexes is not clear. One possible reason could be that the relative width size of the major groove (varies from 7.6 to 9.6 Å) and the minor groove (8.9−10.2 Å) of the DNA·RNA are different from DNA·DNA duplexes (10.5−11.5 Å and 3.4−7.4 Å, respectively).[42] This may mean two things: (i) The Ru^{2+} complex with ∼10 Å diameter is bulky and cannot place itself in the minor or in the major groove of the DNA·RNA duplexes. (ii) On the other hand, DNA·RNA has a minor groove width larger than the DNA·DNA duplex; still the Ru^{2+} complex does not bind there, and the likely reason is most probably that it is a major groove binder. This is indirectly supported by Barton's NMR work[38] in which she showed that the intercalation site of the $[Ru(phen)_2dppz]^{2+}$ complex is indeed in the major groove of DNA·DNA duplex.

(VIII) DNase I Footprinting of (Ru^{2+}-ODN)·DNA Duplexes. The 5′-end of the target DNA strand **13** was 5′-^{32}P-labeled by γ-^{32}P-ATP and T4 polynucleotide kinase. Typical DNase I digestion patterns for all (Ru^{2+}-ODN)·DNA duplexes were compared with the middle-modified (dppz-ODN)·DNA **12′·13** and the native DNA·DNA duplexes (Figures 9−11). The information provided by DNase I digestion are two-fold: (i) The comparison of cleavage yields showed how the structures of (Ru^{2+}-ODN)·DNA duplexes are different from the native unmodified counterpart. (ii) The comparison of the cleavage sites showed where the $[Ru(phen)_2dppz]^{2+}$ complex is intercalated. The ability of the native and (Ru^{2+}-ODN)·DNA duplexes to be a substrate for DNase I decreases from the native (97%) ∼3′-Ru^{2+}-modified (98%) > middle-Ru^{2+}-modified (48%) > 5′-Ru^{2+}-modified (38%) duplex, which are correlated in the opposite order with their thermal stabilities. The extent of the cleavage reflects how deeply (Ru^{2+}-ODN)·DNA duplex structure is altered from the B-form duplex, which is ideal for DNase I recognition.[43] Two main conclusions can be made from this observation: (i) all (Ru^{2+}-ODN)·DNA duplexes are substrates for DNase I, which means that their global duplex conformation is more similar to the B-type DNA·DNA duplex,

(42) Zamaratski, E.; Pradeepkumar, P. I.; Chattopadhyaya, J. *J. Biochem. Biophys. Methods* **2001**. In press.

(43) Suck, D.; Oefner, C. *Nature* **1986**, *321*, 620−625.

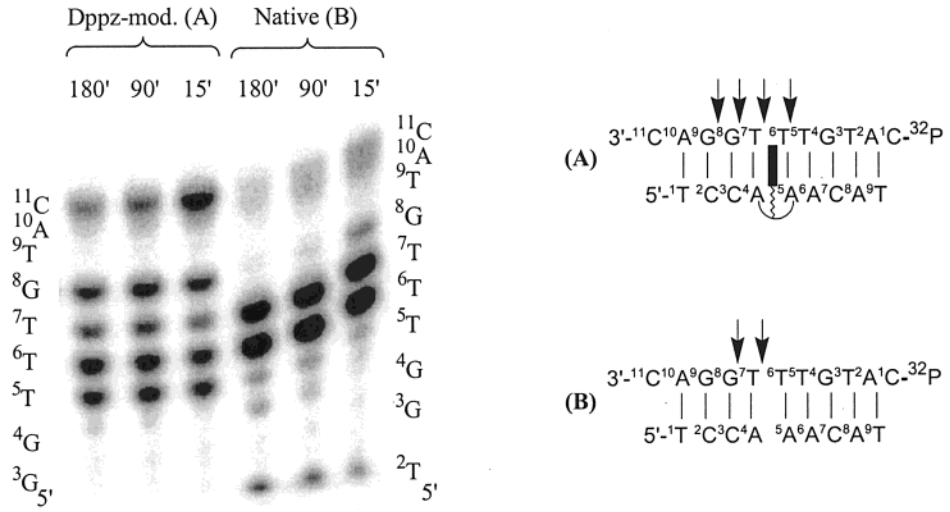

Figure 9. DNase I digestion of duplexes formed from 5′-^{32}P-labeled 11mer **13** and internally modified dppz conjugate **12′** (A) or the native 9mer **9** (B). Time in minutes after the addition of the enzyme is shown at the top of each gel lane. The length and sequence of 5′-^{32}P-labeled ODNs formed upon cleavage are shown on the extreme left and right sides of the gel, and the main cleavage sites after 90 min of reaction are also shown by arrows on the duplex sequence.

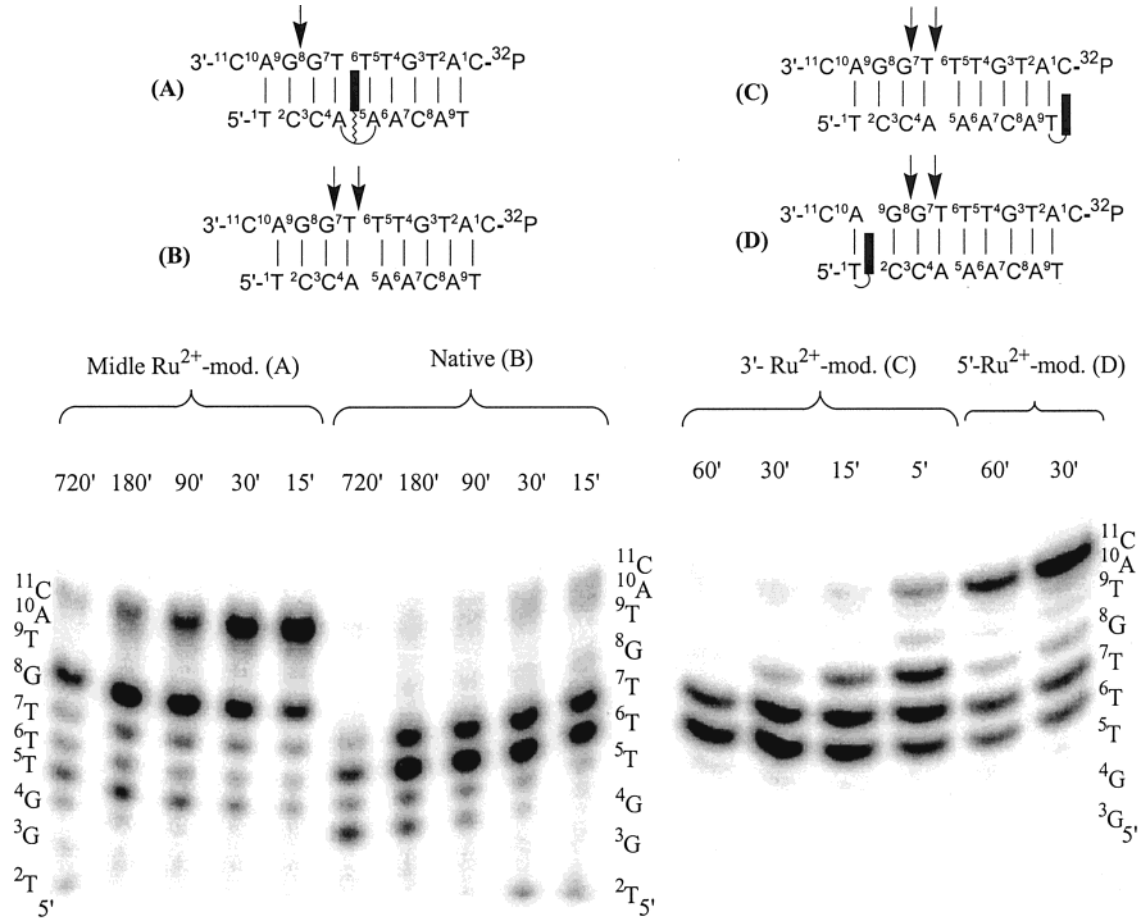

Figure 10. DNase I digestion of duplexes formed from 5′-^{32}P-labeled 11mer **13** with the native 9mer **9** (B) or racemic Ru^{2+}-modified ODNs **10**−**12** (A, C, D). Time in minutes after the addition of the enzyme is shown at the top of each gel lane. The length and sequence of 5′-^{32}P-labeled ODNs formed upon cleavage are shown on the extreme left and right sides of the gel, and the main cleavage sites after 30 min of reaction are also shown by arrows on the duplex sequence.

and the fact that (ii) the 5′- and middle-Ru^{2+}-conjugated duplexes are least degraded (38% and 48%, respectively) suggests that they have undergone major conformational reorganization and distortion from the B-type DNA duplex structure, caused by metallocomplex moiety.

DNase I is known to bind at least 4bp to the 5′-end and 6bp to the 3′-end from the scissile phosphodiester bond[43] of the substrate duplex. Inspection of the cleavage pattern of the 11mer in the native duplex leads us to conclude that the whole duplex should be covered by DNase I. Digestion of the native duplex

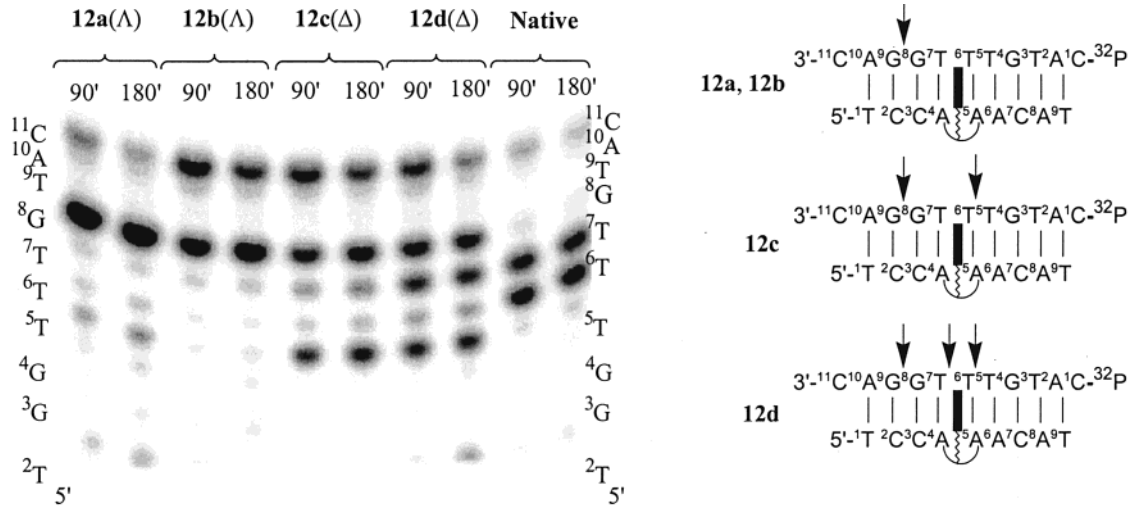

Figure 11. DNase I digestion of duplexes formed from 5′-^{32}P-labeled 11mer **13** with the native 9mer **9** or different diastereomers of Ru^{2+} middle-modified ODNs **12a**−**12d**. Time in minutes after the addition of the enzyme is shown at the top of each gel lane. The length and sequence of 5′-^{32}P-labeled ODNs formed upon cleavage are shown on the extreme left and right sides of the gel, and the main cleavage sites after 30 min of reaction are also shown by arrows on the duplex sequence.

stops at the 7mer (between **^{7}T** and **^{8}G**) and 6mer (between **^{6}T** and **^{7}T**) (Figures 9−11), which cannot be further cleaved because they are too short for DNase I binding.

Cleavage patterns of the racemic mixtures of 5′- or 3′-ruthenated duplexes (Figure 10) are not distinguishable from the native counterpart, while middle modified analogue has completely different digestion pattern (Figure 11). Comparison of the 5′-modified and native duplex cleavage (Figure 10) shows that the cleavage pattern is basically determined by the conformation of 4−5bp from 5′-^{32}P-labeled duplex termini. For 5′-Ru^{2+}-modification the maximal duplex distortion should be at the 5′-end of 9mer that is opposite to 5′-^{32}P-labeled side, leading to only decrease of the extent of digestion (38%), but without any change of the cleavage pattern. On the other hand, the cleavage pattern of the middle ruthenated duplex has considerably changed as a result of protection of those phosphates by the bulky $[Ru(phen)_2dppz]^{2+}$ moiety against the enzyme active site (E75-H131-H_2O[43]). A comparison of the cleavage pattern of the middle-dppz-modified[21] ODN·DNA duplex (Figure 9) with that of racemic middle-modified (Ru^{2+}-ODN)·DNA duplex (Figure 10) shows that, in the former, the cleavage sites are stretched from **^{5}T** to **^{8}G** (Figure 9), which means that none of these phosphates are protected from DNase I cleavage reaction, whereas in the latter, we have more or less only one cleavage site (between **^{8}G** and **^{9}T**, Figure 10), and the other phosphates are protected. This shows that the Ru^{2+} complex in the racemic middle-modified (Ru^{2+}-ODN)·DNA duplex is most probably located between **^{6}T** and **^{7}T**.

Figure 11 exhibits the results of DNase I digestion for pure diastereoisomers of the middle-modified (Ru^{2+}-ODN)·DNA duplexes, showing the unique diasterospecificity of DNAse I recognition between *R*- and *S*-isomers in both Λ and Δ series. It shows that one of the isomers (either *R* or *S* in both series) is cleaved more efficiently than the other. Three critical observations can be made upon comparison of the digestion results of diastereomerically pure Λ_R-, Λ_S-, Δ_R-, and Δ_S-isomers: (i) There is virtually no difference in the cleavage patterns for Λ_R- and Λ_S-isomers in comparison with the Δ_R- and Δ_S-isomers. This means that Λ_R- and Λ_S-isomers have only one and the same $[Ru(phen)_2dppz]^{2+}$ binding geometry, which is completely protecting the three phosphates in **^{5}Tp^{6}Tp^{7}Tp^{8}G**. (ii) The $[Ru(phen)_2dppz]^{2+}$ complex in **12c**(Δ) has a binding geometry which is more localized near **^{6}Tp^{7}Tp^{8}G**, and it does not protect the **^{5}Tp^{6}T** site. (iii) The $[Ru(phen)_2dppz]^{2+}$ complex in **12d**(Δ) has the binding geometry even more localized at **^{6}Tp^{7}T** and does not protect the neighboring phosphates, that is, **^{5}Tp^{6}T** and **^{7}Tp^{8}G** sites. This implies that there are two types of protection which an intercalating complex can confer to the neighboring phosphates: the steric and the conformational (due to configurational change in the octahedral complex).

Conclusions

(1) The novel type of attachment through the dppz moiety of $[Ru(phen)_2dppz]^{2+}$ complex has been implemented. The complex was covalently linked to the non-nucleosidic *sn*-glycerol-tri(ethylene glycol) fused linker through the dppz ligand, allowing us to prepare ruthenium phosphoramidite **6** and CPG-anchored Ru^{2+} for the multiple machine incorporation of the metal complex to the ODN strand.

(2) All four diastereomers (two Λ- and two Λ-stereoisomers) of internally Ru^{2+}-labeled ODN **12** were separated by means of reversed-phase HPLC. They were subsequently used for spectroscopic and enzymatic studies to understand the modes of intercalation in the DNA duplexes along with 3′ and 5′-ruthenated counterparts.

(3) The 5′-, 3′-, and middle-modified ODNs form duplexes with 11mer DNA target, which are significantly stabilized (ΔT_m = 12.8−23.4 °C) compared with the natural DNA·DNA duplex. The 3′- and 5′-modified ODNs also formed stable hybrid duplexes with complementary RNA, but the middle-modified (Ru^{2+}-ODN)·RNA duplex did not show any improved stability compared to the natural counterpart.

(4) DNase I digestion of pure diastereoisomers of the middle-modified (Ru^{2+}-ODN)·DNA duplexes showed unique diastero-specificity of DNAse I recognition between *R*- and *S*-isomers in both Λ and Δ series (**12a**−**d**). Comparison of the digestion results of diastereomerically pure Λ_R-, Λ_S-, Δ_R-, and Δ_S-isomers showed the relative degree of protection from the DNase I, which the complex confer to the neighboring phosphodiester residues in the duplex. The comparison of the relative cleavage pattern with four pure middle-modified diastereomers showed that both steric and the conformational change in the octahedral $[Ru(phen)_2dppz]^{2+}$ complex have profound influence in the way the DNase I can approach the duplex for the cleavage reaction.

Implication

Synthesis of middle Ru^{2+}-incorporated ODNs using $Ru(bpy)_3$ (bpy = 2,2′-bipyridine),[14] $Ru(bpy)_2phen$,[13] and $Ru(tap)_2dip$ (tap = 1,4,5,8-tetraazaphenanthrene, dip = 4,7-diphenylphenantroline)[11] have so far resulted into no stabilization or destabilization of the duplexes, suggesting that such ruthenium complexes are not simply intercalated in DNA double helix. This is the first report of four diastereomerically pure middle Ru^{2+}-incorporated ODNs and their duplexes, which showed considerable stabilization. These diastereomerically pure Ru^{2+}-modified duplexes have been found to have different well-defined stereochemistry with respect to DNA minor and major grooves. This means that the study of their stereochemistry-dependent energy- and electron-transfer chemistry will be useful in understanding oxidative damage to the DNA double helix. It will be also interesting to probe if the diastereospecific interactions between the tethered Ru^{2+} complex and the DNA double helix actually have any influence in the long-range energy- and electron-transfer processes with DNA as a reactant. These diastereomerically pure model ruthenated duplexes also have the potential be useful to understand donor−acceptor properties via luminescence[44] and transient absorption spectroscopies.[45]

Experimental Section

$[Ru(phen)_2dppz](PF_6)_2$ was synthesized according to ref 18. $[Ru(phen)_3]Cl_2$ was purchased from the Aldrich Chemical Co. Ltd. and transformed to the hexafluorophosphate salt. Dry pyridine was obtained by distillation over 4-toluenesulfonyl chloride. Acetonitrile and dichloromethane were distilled from P_2O_5 under argon. Dimethylformamide and tetrahydrofuran were distilled over CaH_2. Acetone was dried with anhydrous K_2CO_3 and then distilled. The silica gel Merck G60 was used for column chromatographic separations of all of the protected intermediates. Semipreparative RP-HPLC was carried out on Spherisorb 5ODS2 using a Gilson equipment with pump model 303, Manometric Module model 802C and Dynamic Mixer 811B connected to a Dynamax computer program for gradient control. TLC was performed on precoated silica gel F_{254} plates with fluorescent indicator in the following dichloromethane−ethanol mixtures: (A) 95:5 (v/v), (B) 90:10 (v/v), (C) 80:20 (v/v). ^1H NMR spectra (δ scale) were obtained at 270 MHz on a JNM-GX 270 spectrometer with $SiMe_4$ as an internal standard. ^{31}P NMR spectra were obtained at 36 MHz on the same spectrometer using 85% phosphoric acid as external standard. ^{13}C NMR spectra were obtained at 22.5 and 69 MHz in the same solvent using the solvent resonance as the internal standard. Thermal denaturation experiments were performed on a PC-computer interfaced Perkin-Elmer UV/vis spectrophotometer Lambda 40 with PTP-6 peltier temperature controller. The CD spectra were recorded using a JASCO J41-A spectropolarimeter. Dioxyribonuclease I from bovine pancreas was purchased from Sigma.

$[Ru(phen)_2(dppz')](PF_6)_2$ (5). Compound **3** (745 mg, 0.69 mmol) and the appropriate amine **4** (182 mg, 0.37 mmol) were coevaporated with dry pyridine separately. The complex **3** was dissolved in dry pyridine (12 mL), and *N*,*N*′-carbonyldiimidazole (169 mg, 1.04 mmol) was added to the solution. The mixture was stirred under nitrogen atmosphere for 2.5 h. Subsequently, a pyridine solution of **4** (6 mL) was added to the reaction mixture under stirring. The reaction mixture was then left stirring at room temperature for 2 days. Pyridine was concentrated ,and the residue was worked up with aqueous saturated $NaHCO_3$ and dried over $MgSO_4$. After evaporation of solvent the residue was coevaporated with toluene and then CH_2Cl_2. The product was isolated by silica gel column chromatography, eluting with 0−5% EtOH in CH_2Cl_2 to give a red foam (358 mg, 57% from amine **4**). R_f: 0.73 (C), 0.27 (A). ^1H NMR (acetone-d_6): 9.72, 9.66 (2H, 2•d, H_γ, $J_{\gamma,\beta}$ = 8.2), 8.94 (1H, s, H_δ), 8.82 (4H, d, $H_{4,7}$, $J_{4(7),3(8)}$ = 8.4), 8.62−8.59 (2H, m, H_2), 8.54−8.50 (4H, m, $H_{\alpha,\epsilon,\lambda}$), 8.43 (4H, s, $H_{5,6}$), 8.40 (2H, d, H_9, $J_{9,8}$ = 4.2), 8.00−7.72 (2H, m, H_β), 7.82 (4H, dd, $H_{3,8}$, $J_{3(8),4(7)}$ = 8.4, $J_{3(8),2(9)}$ = 4.2), 7.39−7.07 (9H, m, DMTr), 6.73−6.69(4H, m, DMTr), 4.00−3.90 (1H, m, $DMTrOCH_2CH$), 3.83−3.64 (20H, overlapping m), 3.22 (2H, d, $DMTrOCH_2$). MS calculated for $C_{73}H_{63}N_9O_8RuP_2F_{12}$ (including ^{102}Ru isotope): 1585.0. Found: 1584.9 ± 0.2.

Phosphoramidite of the $[Ru(phen)_2(dppz')](PF_6)_2$ (6). Compound **5** (214 mg, 0.14 mmol) was coevaporated with dry CH_3CN twice and dissolved in dry CH_3CN (3.4 mL) and kept under N_2. Then dry diisopropylethylamine (87 mg, 0.68 mmol) was added, followed by addition of 2-cyanoethyl diisopropylphosphoramidochloridite (108 mg, 0.46 mmol) under vigorous stirring, which was continued for a further period of 3 h. The reaction mixture was worked up with aqueous saturated $NaHCO_3$, dried over $MgSO_4$, and coevaporated with toluene and then CH_2Cl_2 to afford the ruthenium phosphoramidite **6** (226 mg, 94%), which was then directly dissolved in 1 mL of anhydrous CH_3CN for immediate synthesizer use. R_f: 0.34 (A); ^{31}P NMR ($CDCl_3$): +149.51 and 149.44 ppm.

Succinate of the $[Ru(phen)_2(dppz')](PF_6)_2$ (7). Compound **5** (144 mg, 0.09 mmol) and 4-(dimethylamino)pyridine (46 mg, 0.38 mmol) were dissolved in dry CH_2Cl_2 (1.5 mL). Then, succinic anhydride (18.5 mg, 0.19 mmol) was added, and the solution was stirred at room temperature for 4.5 h. The reaction mixture was first extracted with 0.1 M citric acid followed by aqueous saturated $NaHCO_3$ solution. The organic phase was dried over $MgSO_4$ and evaporated. The product was used without further purification. Yield 25 mg, 43%. R_f: 0.38 (B).

Preparation of the Ru^{2+}-Functionalized Support. CH_2Cl_2 (0.93 mL) solution of diisopropylethylamine (19 mg, 149.0 μmol) was added to succinate block **7** (132 mg, 78.4 μmol), followed by addition of CH_2Cl_2 solution (0.37 mL) of isobutyl chloroformate (10.7 mg, 78.4 μmol). After stirring for 2 h, a solution of DIPEA (0.34 mL) in dry CH_2Cl_2 (0.87 mL) and 3-aminopropyl-CPG (364 mg) were added to the reaction mixture. The suspension was shaken for 2 h and then filtered and thoroughly washed with CH_2Cl_2 (four times) and diethyl ether (four times). The support was then suspended in dry pyridine (2.9 mL), 4-(dimethylamino)pyridine (59 mg) and acetic anhydride (0.26 mL) were added, and the suspension was shaken for 2 h, after which the suspension was filtered and thoroughly washed with pyridine, CH_2Cl_2 (four times) and diethyl ether (four times) and then vacuum-dried over P_2O_5. DMTr release with acid and measurement at 498 nm showed the loading of 20.9 mmol per 1 g of CPG.

Bis(1,10-phenantroline)((11,12-dihydroxy-3,6,9-trioxadodec-1-yl)-dipyrido[3,2-a:2′,3′-c]phenazine-11-carboxamide)ruthenium(II) Bis-(hexafluorophosphate) (8). Compound **5** (71 mg, 0.05 mmol) was dissolved in CH_2Cl_2 (1 mL), and 80% acetic acid (4 mL) was added to the solution. The mixture was shaken for 10 min and evaporated to dryness. The residue was suspended in water and neutralized with triethylamine. The product was isolated by silica gel column chromatography, eluting with 10−50% EtOH in CH_2Cl_2. Yield 132 mg, 86%. R_f: 0.46 (C). ^1H NMR (acetone-d_6): 9.81, 9.80 (2H, 2•d, H_γ, $J_{\gamma,\beta}$ = 8.2), 9.23 (1H, br.t, N*H*CO), 9.17 (1H, d, H_δ, $J_{\delta,\epsilon}$ = 1.2), 8.93, 8.91 (4H, 2•d, $H_{4,7}$, $J_{4(7),3(8)}$ = 7.8), 8.73−8.67 (4H, m, $H_{2,\epsilon,\lambda}$), 8.63 (2H, d, H_α, $J_{\alpha,\beta}$ = 5.2), 8.54 (4H, s, $H_{5,6}$), 8.50 (2H, d, H_9, $J_{9,8}$ = 5.2), 8.07 (2H, dt, H_β, $J_{\beta,\gamma}$ = 8.2, $J_{\beta,\alpha}$ = 5.2), 7.98−7.90 (4H, m, $H_{3,8}$), 4.25 (1H, quintet, $HOCH_2CH$, J = 4.2), 3.83−3.64 (16H, overlapping m). ^{13}C NMR (acetone-d_6): 167.80 (*C*ONH), 154.85 and 154.73 ($C_{\epsilon,\lambda}$), 153.59 (C_2), 153.18 (C_9), 151.65 and 151.48, 148.06, 143.72, 141.91, 141.61, 141.31, 137.22 ($C_{4,7}$), 136.34, 133.95 and 133.78 (C_λ), 131.24, 130.71, 130.38 and 130.16 (C_α), 129.58 (C_δ), 128.32 ($C_{5,6}$), 127.72 and 127.61 (C_β), 126.36 ($C_{3,8}$), 73.30, 72.20, 70.55, 70.21 ($HOCH_2CH$), 69.98 and 69.90 and 69.87 ($O(CH_2)_2O(CH_2)_2O$), 63.92. The proton and carbon assignments have been made on the basis of $^1H-^1H$ COSY and $^1H-^{13}C$ correlation spectrum. MS calculated for $C_{52}H_{45}N_9O_6RuP_2F_{12}$ (including ^{102}Ru isotope): 1283.0. Found: 1582.4 ± 0.2.

Synthesis, Deprotection, and Purification of Oligonucleotides. All ODNs were synthesized on 1.0 μmol scale with an 8-channel Applied Biosystems 392 DNA/RNA synthesizer using conventional 2-cyanoethyl phosphoramidite chemistry. Modified oligonucleotide **11** was synthesized on modified support containing $[Ru(phen)_2dppz]^{2+}$ chromophore tethered to glyceryl residue through the linker of 12-atoms length. Other ODNs were obtained using standard CPG dT-support. The preparation

(44) Kelley, S. O.; Barton, J. K. *Science* **1999**, *283*, 375.
(45) Stemp, E. D. A.; Arkin, M. R.; Barton, J. K. *J. Am. Chem. Soc.* **1997**, *119*, 2921−2925.

of target ODNs **13** and **14** involved the use of standard CPG dC or C-supports. Phosphoramidite block **6** was dissolved in dry acetonitrile with a final concentration of 0.15 M and used after filtration for solid-phase synthesis with a coupling time of 10 min (25 s for standard nucleoside amidites).

After each synthesis of the protected oligomers, the solid support was transferred directly out from the cassette to a 50 mL RB flask containing 20 mL of concentrated aqueous NH_3 and was shaken for 2 h at 20 °C. After removal of CPG by filtration and evaporation of the filtrate, the residue was redissolved in concentrated aqueous NH_3 and stirred at 55 °C for 17 h. The crude ODNs were purified by reversed-phase HPLC (C18 column) eluting with the following gradient systems: A (0.1 M triethylammonium acetate, 5% MeCN, pH 7.0) and B (0.1 M triethylammonium acetate, 50% MeCN, pH 7.0) and the purity of Ru^{2+}-ODN conjugates were checked by analytical reversed-phase HPLC and denaturing 20% polyacrylamide gel electrophoresis. UV−visible spectrum of each collected Ru^{2+}-ODNs showed the characteristic MLCT absorption band of the complex $[Ru(phen)_2dppz']^{2+}$ at 438 nm and IL transition band at 381 nm. The detritylated oligomers were evaporated and coevaporated with water five times and then directly lyophilized (5 × 1 mL H_2O) to dryness. All ODNs were subsequently sodium exchanged through a column of Dowex-50 Na^+ form.

Concentrations of Ru^{2+}-ODNs were determined, accounting for the contribution to the absorbance at 260 nm from the $[Ru(phen)_2dppz']^{2+}$ moiety itself. This was done by taking the ratio of the area under the UV curve for compound **8** at 238−335 nm to that at 335−580 nm. The absorption of the Ru^{2+}-labeled oligomers at 260 nm was then corrected for metal complex absorption at this wavelength by using the above ratio (1.8) for estimation of contribution of Ru^{2+} complex to the absorbance area for a given oligo at 235−335 nm. Starting from 1 μmol of thymidine or complex **8** residues linked to controlled pore glass the following amounts measured in A_{260} units (OD) were obtained after purification: 12 of **10**; 67.7 of **11**; 1.2 of **12a**; 6.9 of **12b**; 15.4 of **12c**.

Enzymatic Digestion of Middle-Modified ODN. ODN (∼1 nM) and SVP (∼1 nM) or spleen phosphodiesterase (1 mg/mL) was incubated in H_2O without the addition of salts and buffer at room temperature for 5 min. The sample was then added to matrix solution for MALDI-TOF-MS.

Thermal Denaturation Experiments. UV melting profiles were obtained by scanning A_{260} absorbance versus time at a heating rate of 1.0 °C/min from 10 to 70 °C. The melting temperature, T_m (±0.5 °C), was determined as the maximum of the first derivative of melting curves. The duplex melting experiments were performed in 1.3 mL of buffer I (20 mM Na_2HPO_4/NaH_2PO_4, 0.1 M NaCl at pH 7.3) at hybrid concentration of ∼1 μM. The approximate extinction coefficients for natural ODNs were calculated as previously described.[46,31] In cases of the Ru^{2+}-tethered ODNs, the extinction coefficients were corrected for the absorbance contribution of the $[Ru(phen)_2dppz']^{2+}$ moiety at 260 nm by subtraction. After preparation, the solutions consisting of two components (for forming of duplexes) were heated to 70 °C for 5 min, and then allowed to cool to 20 °C for 30 min under shaking. During the melting measurements at temperatures below ∼15 °C, nitrogen gas was continuously passed through the sample compartment to prevent moisture condensation.

Circular Dichroism Spectra. CD spectrums of Ru^{2+}-labeled ODNs and their duplexes were recorded from 550 to 220 nm, and CD spectrums of natural 9mer and its duplex were recorded from 320 to 220 nm. All CD experiments were performed in 0.2 cm path length cuvettes using 8 μM strand concentration in 650 μL of buffer II (20 mM Na_2HPO_4/NaH_2PO_4, 1 M NaCl at pH 7). For CD spectra of duplexes the temperature was maintained at 5 °C by circulating thermostated water through the cuvette holder, while for single-stranded ODNs it was maintained at 5 and 55 °C. The samples were equilibrated at the required temperature for 10 min before recording the spectra. Each spectrum was an average of two scans with the buffer blank subtracted, which was recorded at the same sensitivity (0.2, 0.5, or 2 m°/cm) and scan speed (10 or 20 nm/min). The time constant used were 16 s. Each point in the spectra was manually fed into the SigmaPlot 2000 software in a PC.

DNase I Footprinting. A 10 μL solution containing buffer (100 mM Tris, 10 mM $MgCl_2$ at pH 7.5), 10 μM of duplex, and 20 000 cpm of 5′-^{32}P-labeled 11mer **13** was heated to 70 °C for 5 min, and then allowed to cool to 20 °C for 45 min. Cleavage was initiated by the addition of 1 μL of 1.33 unit/μL DNase I, 150 mM NaCl, 1 mM $MgCl_2$ and allowed to react at room temperature before addition of a formamide loading buffer. The mixture was then loaded onto 20% polyacrylamide/7M urea gel and electrophoresed at 700 V for 2 h. DNA fragments were visualized by Molecular Dynamics phosphorimager.

Acknowledgment. We thank the Swedish Natural Science Research Council (NFR) and Swedish Engineering Research Council (TFR) for generous funding. We also thank Dr. P. Lincoln and Professor B. Nordén for providing us with the experimental protocol for ruthenium complex.

JA003985T

(46) Sund, C.; Puri, N.; Chattopadhyaya, J. *Tetrahedron* **1996**, *52*, 12275−12290.